ORIGINAL ARTICLE

DOI: https://doi.org/10.18599/grs.2021.4.10 Russian Original 2021. Vol. 23. Is. 4. Pp. 80–95

On the melt differentiation in the intermediate chamber (by the example of differentiated intrusives of the western slope of the Southern Urals)

S.G. Kovalev[*], *S.S. Kovalev*

Institute of Geology – Subdivision of the Ufa Federal Research Centre of the Russian Academy of Sciences, Ufa, Russian Federation

Abstract. The article provides materials on the analysis of the chemical composition of silicates and aluminosilicates that make up the differentiated body of the Misaelga complex, which made it possible by calculation methods to restore the thermobaric parameters of crystallization of the melt in the intermediate chamber.

The presence of high-temperature (1472 ºC) intratelluric olivine crystals characterizing the process of magma generation in the mantle and olivine crystallizing under the conditions of the intermediate chamber (1050–1183 ºC) has been established. The calculated crystallization temperature of pyroxenes indicates that they crystallized together with olivine from the bulk of the rocks, and the established variations in the P–T parameters (T = 950–1045 ºC, P = 4.0–7.4 kbar) for plagioclase and amphibole complete the quantitative characteristics of high-temperature melt crystallization processes.

It is shown that the calculated P–T parameters of the crystallization of the melt that formed the intrusive massif make it possible to classify its ultrabasic horizon as picrite complexes of the second type that we identified earlier.

Modeling of the crystallization process carried out using two models – according to the algorithm of H.D. Nathan and K.K. Van Kirk and the software product KOMAGMAT – made it possible to establish that the most probable mechanism for the formation of a differentiated body of the Misaelga complex was directional crystallization with gravitational deposition of olivine at the initial stages of the formation of the massif.

Keywords: Southern Urals, differentiated body, olivine, clinopyroxene, orthopyroxene, modeling, crystallization temperature, melt differentiation, liquidus phases

Recommended citation: Kovalev S.G., Kovalev S.S. (2021). On the melt differentiation in the intermediate chamber (by the example of differentiated intrusives of the western slope of the Southern Urals). *Georesursy = Georesources*, 23(4), pp. 80–95. DOI: https://doi.org/10.18599/grs.2021.4.10

Introduction

The processes of material differentiation during the formation of magmatic rocks of basic-ultrabasic composition have been studied for about 100 years, since the pioneering work of Bowen (1928) and the classical studies of L.P. Wager and G. Brown (Wager, Brown, 1970). The quantitative physicochemical study of magmatic processes began with experimental studies of binary and ternary silicate systems with a limited set of components. The interpretation of equilibria with the participation of natural melts was carried out mainly by means of projections of magma compositions onto the phase diagrams of simplified systems. The laboratory-experimental and analytical base, improved in recent years, has made it possible to significantly change these views, which was expressed in an snowballing number of publications devoted to experiments on melting and crystallization of rocks under different P-T conditions and with different amounts of components.

In the second half of the 20th century and the beginning of the 21st century, numerous models were developed that calculate the crystallization temperatures of silicate minerals, the order of their separation and the behavior of the residual melt (Roedder, Emslie, 1970; Nathan, Vankirk, 1978; Nielsen, 1985, 1988; Ariskin et al., 1986, 1993; Frenkel et al., 1988; Beattie, 1993; Ariskin, Barmina, 2000 and many others). Further development of the models was aimed at studying the behavior of trace elements and isotope ratios in magmatic systems during partial melting, fractional crystallization, mixing of magmatic melts, contamination of crustal material in combination with fractional crystallization (DePaolo, 1981; Powell, 1984; Aitcheson, Forrest, 1994; Bohrson, Spera, 2001, 2002; Spera, Bohrson, 2001, 2002, 2004; Bychkov, Koptev-Dvornikov, 2005).

[*]Corresponding author: Sergey G. Kovalev
E-mail: kovalev@ufaras.ru

Despite the large number of publications devoted to the problem of material differentiation during the formation of igneous rocks (Namur et al., 2010; Humphreys, 2011; Toramaru, Matsumoto, 2012; Leuthold et al., 2014; Gillis et al., 2014; Layered Intrusions, 2015; Erofeeva et al., 2019 and many others), a significant problem, from our point of view, is represented by a limited number of real geological objects that are used (or can be used) to verify the developed software products. The purpose of this work is an attempt to consider the mechanism of melt differentiation in the intermediate chamber using the extensive author's material using the example of differentiated bodies of the Misayelga complex located on the western slope of the Southern Urals.

Research methods

The section of the intrusive bodies was studied using the borehole core samples. Minerals were studied using a scanning electron microscope REMMA-202M with an LZ-5 X-ray energy-dispersive spectrometer (SiLi detector, resolution 140 eV) and detectors of secondary (SE) and reflected (COOMPO) electrons at the Institute of Mineralogy, Ural Branch of the Russian Academy of Sciences (Miass, analyst V.A. Kotlyarov). When carrying out a quantitative analysis at a point, an accelerating voltage of 20–30 kV was used at probe currents from 4 to 6 nA. When analyzing the composition of minerals, pure metal standards (Micro-Analysis Consultants LT, LTD, X-RAY Microprobe standards, Registered Standard Number 1362) or synthetic (or natural) mineral standards (Astimex Scientific Limited, MINM 25-53, Mineral Mount Serial No: 01-044).

Research results

The Misayelga complex is represented by two differentiated ferrogabbro-dolerite-picrite bodies found in the southwestern part of the Taratash metamorphic complex located in the West Ural megazone (Alekseev, 1984; Kovalev, 1996). To date, the age of these bodies is based on the K-Ar method – 780 Ma (Lennykh, Petrov, 1978) and Rb-Sr method – 726 ± 13 Ma (Kovalev, 1996).

The intrusive massifs form bodies that are gently dipping to the west, 45 m and more than 216 m thick (Fig. 1). They are composed of olivine dolerites, porphyry-like picrodolerites (both varieties in subordinate amounts in the endocontact zones), medium-grained picrites and picrodolerites, gabbro-dolerites and ferrogabbro-dolerites.

When carrying out a detailed petrographic study in a large intrusion, the following horizons were identified (from bottom to top): the lower endocontact zone ~ 1.0–1.5 m thick, picrite horizon – ~ 110–112 m, gabbro horizon – 100–110 m.

The lower endocontact zone is composed of olivine dolerites and porphyry picrodolerites. In appearance,

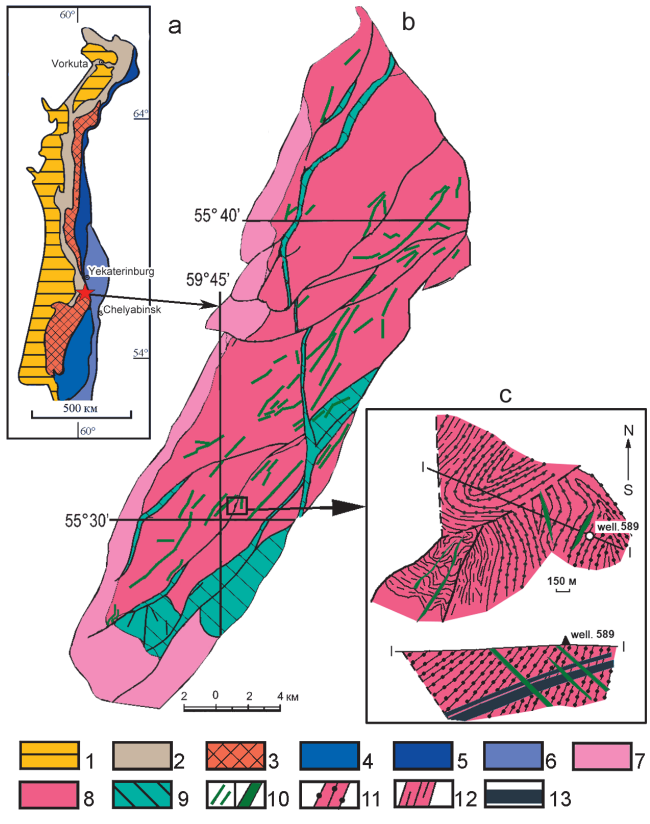

Fig. 1. Structural diagram of the Urals (a), geological diagram of the Taratashsky complex (b) and the «Magnitny» site with rock bodies of the Misayelga complex (c). Megazones of the Urals: 1 – Pre-Ural; 2 – West Ural, 3 – Central Ural, 4 – Tagil, 5 – Magnitogorsk, 6 – East Ural; 7 – deposits of the Aisk suite (RF_1); 8 – undivided Archean-Proterozoic deposits; 9 – tectonic zones with blastomylonites; 10 – mafic dikes of different ages; 11 – migmatites; 12 – garnet-biotite gneisses; 13 – layered bodies of the Misayelga complex

they are dark (to black), dark green rocks with a medium-grained porphyry structure and massive texture. The mineral composition includes: olivine, orthopyroxene, clinopyroxene, plagioclase, brown hornblende, biotite, magnetite, titanomagnetite, ilmenite, sulfides, apatite, titanite.

The picrite horizon is represented by dark gray massive, medium-grained picrites, the microstructural features and mineral composition of which change (gradually) depending on the location in the section. The lower part is characterized by poikilitic structures, which often contain accumulations of olivine, forming glomeroporphyric segregations (Fig. 2).

Further up the section, the structures become hypidiomorphic-granular with porphyric elements. Orthopyroxene crystals act as porphyry phenocrysts. The change in the mineral composition from bottom to top along the section consists in a regular decrease in the amount of olivine and orthopyroxene. The composition of the rocks includes olivine (10–20 %), orthopyroxene (10–20 %), clinopyroxene (30–40 %), plagioclase (10–20 %), biotite (2–3 %), magnetite

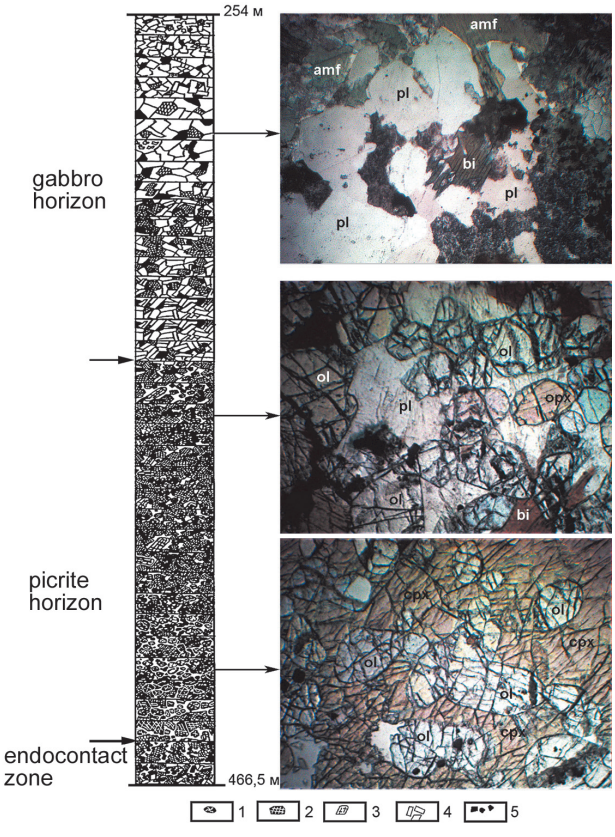

Fig. 2. Petrographic section and micrographs of rocks of the Misayelga complex: ol – olivine; opx – orthopyroxene; cpx – clinopyroxene; pl – plagioclase; amf – amphibole; bi – biotite. 1 – olivine; 2 – clinopyroxene; 3 – orthopyroxene; 4 – plagioclase; 5 – ore minerals

(2–3 %), ilmenite (picroilmenite) (1–2 %), chrome spinel (chrome magnetite) (1–2 %), chalcopyrite (0–2 %), pyrrhotite (0–2 %), pentlandite (0–2 %). The association of secondary minerals consists of actinolite, serpentine, talc, chlorite, sericite, carbonate, and fine magnetite.

The gabbro horizon is composed of bipyroxene gabbros, ferrogabbro-dolerites, their more leucocratic varieties (Fig. 2) to vein plagiogranites. The structures of the rocks vary from porphyritic to ophitic, hypidiomorphic-grained – gabbro (in veinlet plagiogranites – hypidiomorphic-grained, granite). The mineral composition includes clinopyroxene (40–45 %), orthopyroxene (0–5 %), plagioclase (40–45 %), amphibole (10–15 %), biotite (3–5 %), magnetite (3–5 %) , titanomagnetite (5–10 %), sulfides (1–3 %) (with a predominance of pyrite). The association of secondary minerals is represented by amphibole (green hornblende, actinolite), albite, sericite, epidote, chlorite, talc, titanite, magnetite, and leucoxene.

In the upper parts of the body, there is a veinlet of plagiogranite composition 5–8 cm thick, composed of plagioclase No. 4–46 (from albite to andesine) in an amount of up to 40–60 %, sericite, magnetite, apatite, and quartz, which is the most acidic derivative of magma that formed intrusive.

Olivine is represented by crystals of two generations. The first (early) includes segregations 0.8–1.3 mm in size, having a zonal structure, the central parts of which correspond to 88 Fo, and the marginal parts correspond to 73 Fo. In the bulk of rocks, the mineral is represented by idiomorphic crystals 0.3–1.0 mm in size. Its content ranges from single crystals in the lower zone to 10–20 % in the central parts of the picrite horizon. Olivine of the second generation often forms glomeroporphyric accumulations and intergrowths; its crystals are overgrown with ortho- and clinopyroxene, as well as poikilitic inclusions in the latter. The mineral contains a constant admixture of MnO (from 0.1 to 0.57 wt- %) and NiO (from 0.09 to 0.62 wt- %) (Table 1).

In addition, latent stratification is observed, which consists in a decrease in the forsterite endmember when moving from the bottom up along the body section. Calculations of the crystallization temperature performed using an olivine-clinopyroxene geothermometer (Loucks, 1996) showed that $T_{crystal.}$ of olivine varies within the range from 1050 ºC to 1183 ºC from the bulk of the rocks, while in the central parts of relatively large porphyritic segregations it is 1472 ºC (Table 1).

Figure 3 shows the dependences of the contents of FeO, SiO_2, NiO, and MnO on the amount of forsterite end-member in olivines from picrite and picrodolerite complexes also occurring in the form of sills, sheet intrusions and dikes on the western slope of the Southern Urals, materials on which were borrowed from published works (Kovalev, 2011; Sazonova et al., 2011; Nosova et al., 2012; Kovalev et al., 2018). Analysis of the obtained material allows us to draw the following conclusions:

- On the Fo-FeO and Fo-SiO_2 diagrams, the maximum scatter of the contents of these components characterizes the chemical composition of olivines in the picrites of the western slope of the Southern Urals, while the olivines of the Misayelga complex occupy a well-defined interval of this sequence (67.4–76.1 Fo), characterizing the melt from which they formed, and its similarity / difference from analogues. In addition, it is important to note that the point corresponding to the center of the crystals (87.7 Fo) is cut off from the sequence, which may serve as evidence of the intratelluric nature of these formations;

- As established by L.H. Fuchs with colleagues, the modal NiO content in olivine of mantle rocks is 0.4 wt- % (Fuchs et al., 1973). It can be seen from the Fo-NiO diagram (Fig. 3) that most of the figurative points of the olivines from the Lysogorsk and Ishla complexes, as well as the point characterizing the center of olivine crystals from the Misayelga complex, are grouped around a value of 0.4 wt- % NiO, while for olivine in the bulk of rocks from the Misayelga complex, the scatter of values ranges from below the detection limit of the method to 0.62 wt- %. In (Campbell, Roeder, 1968), the effect of oxygen fugacity on the incorporation of

No.	SiO_2	Al_2O_3	FeO	MnO	MgO	NiO	Total	Fo	T, C°
1	37.52	bdl	27.8	0.47	33.71	bdl	99.5	68.3	1050.1
2	37.41	0.11	28.48	0.49	33.02	0.09	99.6	67.4	1069.9
3	37.42	0.07	27.28	0.42	33.93	0.43	99.55	68.9	1072.4
4	37.35	bdl	27.69	0.57	34.03	bdl	99.64	68.6	1115.9
5	37.92	bdl	27.04	bdl	34.63	bdl	99.59	69.5	1134.7
6	36.89	bdl	27.89	0.54	34.1	0.24	99.66	68.5	1138.5
7	38.59	0.05	22.77	0.2	37.79	0.47	99.87	74.7	1167.8
8	38.52	0.13	23.33	0.1	37.6	0.3	99.98	74.1	1183.9
9	38.78	bdl	22.53	0.19	37.88	0.25	99.63	74.9	–
10	38.25	bdl	22.51	0.37	38.14	0.23	99.59	75.1	–
11	38.33	0.08	21.85	0.45	38.47	0.46	99.64	75.8	–
12	38.49	0.01	21.57	0.27	38.65	0.62	99.61	76.1	–
13	38.05	0.05	23.0	0.32	37.51	0.51	99.44	74.3	–
14	38.36	0.09	23.26	0.43	36.87	0.37	99.38	73.8	–
15	37.95	0.06	23.78	0.48	36.96	0.46	99.69	73.4	–
16	37.79	0.1	23.73	0.43	37.09	0.31	99.45	73.5	–
17	38.48	bdl	21.72	0.36	38.26	0.35	99.17	75.8	–
18	38.43	bdl	23.32	0.17	37.42	0.22	99.56	74.1	–
19	38.01	bdl	23.65	0.36	37.1	0.43	99.55	73.6	–
20	37.77	bdl	24.5	0.19	36.65	0.25	99.36	72.7	–
21	38.6	bdl	22.08	0.18	38.25	0.22	99.33	75.5	–
22	37.92	bdl	25.59	0.46	35.54	0.3	99.81	71.2	–
23	37.42	0.1	27.15	0.46	34.18	0.3	99.61	69.1	–
24	37.26	bdl	25.84	0.43	35.66	0.36	99.55	71.1	–
25	40.35	bdl	11.7	0	46.89	0.46	99.4	87.7	1472.3

Tab. 1. Chemical compositions of olivine from rocks of the Misayelga complex (wt- %). Numbers 1–24 are groundmass olivine, and No. 25 is phenocryst. In No. 9, 0.09 wt- % Cr_2O_3. Hereinafter, bdl – below detection limit.

nickel into olivine was established. In parallel with the oxidation of iron in olivine and the removal of Fe^{3+} from it, the mineral is enriched with nickel. In addition, a decrease in the content of NiO and fayalite molecules in olivine may be associated with an increase in sulfur fugacity, leading to the removal of Ni and the formation of pentlandite. Thus, all variations in the NiO content in the "Misaelga" olivines could be due to the process of intrachamber differentiation with varying physicochemical parameters of the melt;

- The amount of MnO in olivines from picrites of all complexes is subject to significant fluctuations; The least manganese are olivines from the rocks of the Ishlinsky complex, and the maximum contents and scatter of values (below the detection limits – 0.27 wt- %) are characteristic of olivines from the rocks of the Misayelga complex (Fig. 3). According to M. Miyamoto et al. (1993), the content of manganese and iron in olivine is associated with the redox conditions of mineral formation, and the positive correlation between Mn and Fe characterizes the temperature conditions of olivine formation. In our case, there is a direct correlation between these components, which, just like the nickel content, indicates the dependence of the variations of impurity elements in olivine on the process of intrachamber differentiation of the melt.

In our case, there is a direct correlation between these components, which, just like the nickel content, indicates the dependence of the variations of impurity elements in olivine on the process of intrachamber differentiation of the melt (De Hoog et al., 2010).

Clinopyroxene crystals in general determine the porphyritic appearance of the rocks of the picrite horizon. Its amount, as well as the size of individual crystals, increases from bottom to top along the section (content – from 25 to 30–40 %, sizes – from 0.6 to 1.2 mm). The form of the discharge varies from xenomorphic to idiomorphic. Very often, its crystals form glomerocrystalline and glomeroporphyric intergrowths. In the gabbro horizon, clinopyroxene is represented by prismatic idiomorphic and subidiomorphic to xenomorphic crystals, forming, together with plagioclase, gabbro and dolerite rock structures. The chemical composition of clinopyroxene is shown in Table 2.

On the classification diagram (Fig. 4), all clinopyroxene compositions are grouped in the augite field at the border with its magnesium variety.

The rocks contain zonal crystals, in which the central parts are depleted in comparison with the marginal ones – SiO_2, TiO_2, MgO, CaO, Na_2O and are enriched in FeO and Al_2O_3. Despite the relatively local field, which is formed by the points of the clinopyroxene compositions on the Mg-Ca-Fe diagram (Fig. 4), there are noticeable differences between the chemical compositions of minerals from the picrite and gabbro horizons (hidden layering). In particular, the former contains more TiO_2 average. (0.62 and 0.16 wt- %, respectively), Al_2O_3 average. (2.47 and 1.41 wt- %), MgO aver. (15.25 and

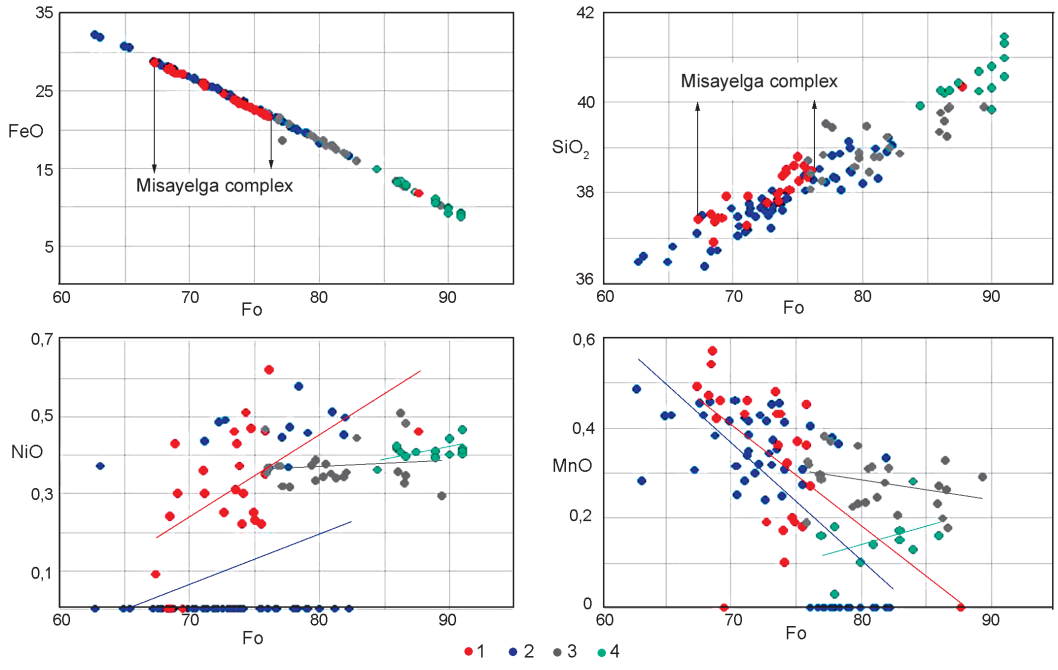

Fig. 3. Binary diagrams for olivines from picrite and picrodolerite complexes of the western slope of the Southern Urals: 1 – Misaelga complex; 2 – picrites of borehole # 7; 3 – Lysogorsky complex (Nosova et al., 2012); 4 – Ishlinsky complex. Colored lines are trends.

13.27 wt- %), Na_2O average (0.47 and 0.38 wt- %) and less FeO average. (7.24 and 9.63 wt- %), CaO average (20.29 and 21.51 wt- %) and MnO average (0.03 and 0.11 wt- %). In addition, the clinopyroxenes from the picrite horizon contain a constant admixture of Cr_2O_3 (from 0.11 to 0.69 wt- %), which is absent in analogs from the gabbro horizon (Table 2).

The results of a comparative analysis of clinopyroxenes from the characterized rocks with analogs from picrite and picrodolerite complexes of the western slope of the Southern Urals (Fig. 5) can be summarized as follows:

- In the direction from gabbroids to picrites in clinopyroxene, the amount of titanium, chromium, aluminum and sodium increases with a decrease in iron and calcium, which characterizes the normal process of intracameral differentiation;

- As in the case of olivine, clinopyroxene from picrites of the Misayelga complex is close in all respects to analogs from picrites from borehole no. 7 (Sazonova et al., 2011) and picrites and picrodolerites of the Lysogorsk complex, differing significantly from clinopyroxene from picrites of the Ishlinsky complex (Sazonova et al., 2011) in the MgO content, which indicates, first of all, the similarity / differences in the chemical composition of melts and the conditions for their generation;

- The analogs from gabbroids and pyroxenites of the Kusinsko-Kopansky intrusive complex complex (Sazonova et al., 2011) are the closest in almost all the parameters under consideration to clinopyroxenes of the Misayelga complex, which, in our opinion, is of fundamental importance.

Orthopyroxene is present in the rocks of the picrite horizon in an amount of 3–8 %, in the lower gabbro horizon – 1–3 %. The mineral is represented by elongated idiomorphic prisms, elongated from 2–3 mm to 6.0–6.5 mm, pleochroic in pinkish-greenish tones. Orthopyroxene overgrowth of olivine is often observed, as well as large chadacrysts with poikilite-included oicocrystals of olivine and clinopyroxene (Fig. 2). Its chemical composition contains impurities of TiO_2 (from 0.1 to 0.64 wt- %), Al_2O_3 (from 0.5 to 2.39 wt- %), Cr_2O_3 (from 0.08 to 0.69 wt- %), MnO (from 0.07 to 0.21 wt- %), Na_2O (from 0.1 to 0.44 wt- %), K_2O (from 0.03 to 0.1 wt- %) (Table 3). A constant CaO admixture (from 0.31 to 2.35 wt- %) Makes it possible to diagnose orthopyroxene as clinoenstatite (Fig. 4). The average crystallization temperature calculated using two-pyroxene geothermometers (Wood, Banno, 1973; Wells, 1977; Perchuk et al., 1977; Kretz, 1982) is 1071–1073 ºC (Table 4) and indicates that pyroxenes crystallized together with olivine of the bulk of the rocks.

Plagioclase in the picrite horizon is sharply xenomorphic in relation to mafic minerals and fills the interstitial space between them. Only near direct contact with the host rocks does it have a tabular-lath-like shape. Its amount in picrites is 10–30 %. In the gabbro horizon, plagioclase is represented by either wide-tabular crystals or xenomorphic precipitates characteristic of the gabbro structure. Its amount rises to 40–50 %. The chemical composition of plagioclases contains FeO (from 0.11 to 1.84 wt- %) and MgO (from 0.01 to 0.37 wt- %). In addition, all plagioclases contain a potassium impurity ranging from 0.07 to 0.68 wt- % (Table 5), and the composition varies from albite to labradorite.

An interesting feature is observed in the Ab-Or-An diagram (Fig. 6), where the points of the Ab and An abundances in plagioclases from the picrite horizon form a continuous row from albite to labradorite, while for analogs from the gabbro horizon, a relatively clearly manifested break in the area of the border between oligoclase and andesine. Most likely, this feature is the result of differences in the conditions of the crystallization process (crystallization of the intercumulus melt in the first case and the formation in the form of a liquidus phase in the second). In addition, plagioclase albitization as a metamorphic process cannot be ruled out.

Amphiboles are one of the most common groups

No.	SiO_2	TiO_2	Al_2O_3	Cr_2O_3	FeO	MnO	MgO	CaO	Na_2O	Total
1	52.56	0.51	2.41	bdl	8.46	0.1	14.15	20.81	0.51	99.51
2	52.67	0.5	2.67	bdl	9.58	0.11	14.43	19.68	0.18	99.82
3	52.62	0.36	2.17	bdl	8.63	0.08	14.29	20.83	0.48	99.46
4	53.96	bdl	0.62	bdl	8.89	0.15	13.61	21.71	0.41	99.35
5	53.35	0.24	1.73	bdl	8.74	0.15	14.2	20.55	0.54	99.5
6	50.9	bdl	4.07	bdl	13.29	bdl	14.49	16.82	0.26	99.83
7	53.47	0.41	1.97	bdl	8.71	bdl	14.88	19.6	0.55	99.59
8	54.0	0.1	0.81	bdl	8.35	bdl	14.12	21.33	0.55	99.26
9	54.14	0.13	1.24	bdl	8.83	0.07	14.13	20.88	0.28	99.7
10	51.62	0.06	0.84	bdl	12.55	0.18	11.5	22.64	0.24	99.63
11	54.12	bdl	0.45	bdl	9.12	0.13	12.44	23.12	0.53	99.91
12	53.84	bdl	0.26	bdl	7.84	0.1	13.27	23.91	0.31	99.53
13	53.78	bdl	0.24	bdl	8.01	0.26	12.84	24.12	0.42	99.67
14	53.67	bdl	0.98	bdl	9.34	bdl	13.17	21.88	0.45	99.49
15	52.55	bdl	0.3	bdl	11.21	0.27	11.27	23.37	0.06	99.03
16	51.02	bdl	2.97	bdl	11.22	bdl	10.36	23.81	bdl	99.38
17	53.53	bdl	0.71	bdl	12.15	0.27	12.58	19.99	0.33	99.56
18	53.62	bdl	0.37	bdl	7.81	0.14	13.89	23.24	0.27	99.34
19	52.32	0.72	2.81	bdl	8.19	0.07	12.88	21.98	0.85	99.82
20	53.83	bdl	0.74	bdl	7.7	bdl	14.12	22.23	0.54	99.16
21	53.91	bdl	0.41	bdl	7.2	bdl	14.25	23.19	0.54	99.5
22	53.9	bdl	0.72	bdl	8.28	0.15	13.95	22.33	0.29	99.62
23	54.19	bdl	0.43	bdl	7.8	bdl	13.78	22.88	0.05	99.13
24	52.93	bdl	0.33	bdl	7.09	0.11	13.16	23.07	0.57	97.26
25	52.52	0.42	2.51	bdl	1.97	0.1	14.92	19.64	0.27	92.35
26	52.68	0.28	1.94	bdl	8.79	0.13	15.21	20.27	0.29	99.59
27	51.07	0.65	3.12	bdl	8.5	0.06	14.25	20.98	0.6	99.23
28	52.91	0.45	2.25	bdl	7.84	bdl	15.85	19.94	0.23	99.47
29	52.36	0.53	2.84	bdl	8.29	0.11	15.19	20.05	0.14	99.51
30	51.83	0.72	3.67	bdl	7.97	bdl	14.98	20.08	0.34	99.59
31	52.52	0.34	2.54	bdl	8.59	bdl	14.55	20.13	0.52	99.19
32	53.48	0.48	2.08	0.59	6.35	0.03	17.01	18.92	0.61	99.55
33	54.18	0.1	1.63	0.24	6.29	bdl	15.45	20.92	0.72	99.53
34	53.91	0.26	1.53	0.3	5.93	0.06	15.25	21.37	0.73	99.34
35	52.72	0.78	2.78	0.54	7.99	bdl	16.88	17.57	0.46	99.72
36	52.31	0.94	2.62	0.11	7.48	0.15	14.81	20.22	0.56	99.2
37	51.47	1.11	2.87	0.28	7	bdl	13.86	22.24	0.36	99.19
38	53.76	0.23	1.18	bdl	5.68	bdl	16.17	22.04	0.26	99.32
39	52.08	0.95	2.88	0.29	7.97	0.09	15.81	18.44	0.51	99.02
40	53.9	0.3	2.03	0.23	6.47	0.04	15.34	20.95	0.51	99.77
41	52.92	0.62	2.4	0.19	6.81	bdl	15.5	20.57	0.52	99.53
42	52.65	0.7	3.02	bdl	7.18	bdl	16.19	19.76	0.33	99.83
43	50.57	1.73	4.49	0.52	6.64	0.1	15.06	20.24	0.41	99.76
44	51.19	1.57	4.02	0.69	6.66	bdl	14.83	20.27	0.62	99.85
45	52.13	0.94	2.97	bdl	6.3	bdl	16.64	20.09	0.34	99.41
46	51.87	1.03	3.54	bdl	8.09	bdl	15.49	18.79	0.48	99.29
47	52.57	0.87	3.48	bdl	7.12	bdl	15.86	19	0.71	99.61
48	52.11	0.8	3.13	bdl	7.63	bdl	16.2	18.82	0.39	99.08
49	51.51	1.21	4.07	bdl	7.85	bdl	15.43	18.53	0.57	99.17
50	53.54	0.61	2.61	bdl	7.7	bdl	16.1	18.79	0.55	99.9
51	51.99	1.33	4.21	bdl	8.02	bdl	15.91	16.96	1.05	99.47

Tab. 2. Chemical compositions of clinopyroxene from rocks of the Misayelga complex (wt- %). No. 1–19 – gabbro, No. 20–51 – picrites

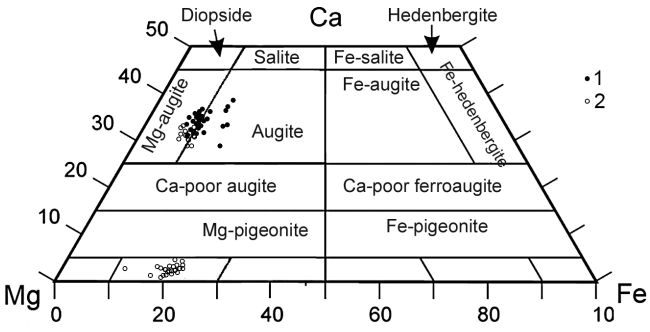

Fig. 4. Classification diagram for pyroxenes from rocks of the Misayelga complex: 1 – pyroxenes of the gabbro horizon; 2 – pyroxenes of the picrite horizon

of minerals present in the rocks of the complex. They are represented by subidiomorphic and idiomorphic crystals ranging in size from 0.5 to 2 mm in length, green, greenish-brown and brown in color, often with pronounced pleochroism and zonal structure (greenish-brown nuclei and light green edges) associated with plagioclase, biotite, and titanite. In addition, amphibole develops after pyroxene to the formation of complete pseudomorphs.

Its composition varies widely (Fig. 7, a). Analysis of the Ca + Al^{IV} – Si + (Na + K) diagram (Fig. 7, b) showed that almost half of the analyzed minerals belong to "early magmatic", located above the line (Ca + Al^{IV}) = 2.5, and the other half – to "late magmatic» formations. Moreover, in gabbroids this subdivision is very clearly manifested (with a break in the "continuity" of the trend), and in the picrite horizon, amphiboles form a continuous sequence. Most likely, in this case we have a genetically continuous series of minerals – magmatic amphibole – autometamorphic amphibole. The amphibole-plagioclase geothermobarometer proposed by J. Blondy and T. Holland (Blundy, Holland, 1990) was used to calculate the thermobaric parameters of amphibole formation under the following conditions: minerals must contact each other; the sum of Ca + Na + K in amphibole should be in the range of 2.3–2.9 f.c. As a result of calculations, temperature and pressure variations were obtained: T = 950–1045 ºC, P = 4.0–7.4 kbar.

Biotite is distributed throughout the body section in the form of wide-tabular crystals with clear pleochroism in brownish-fulvous tones. The mineral is characterized

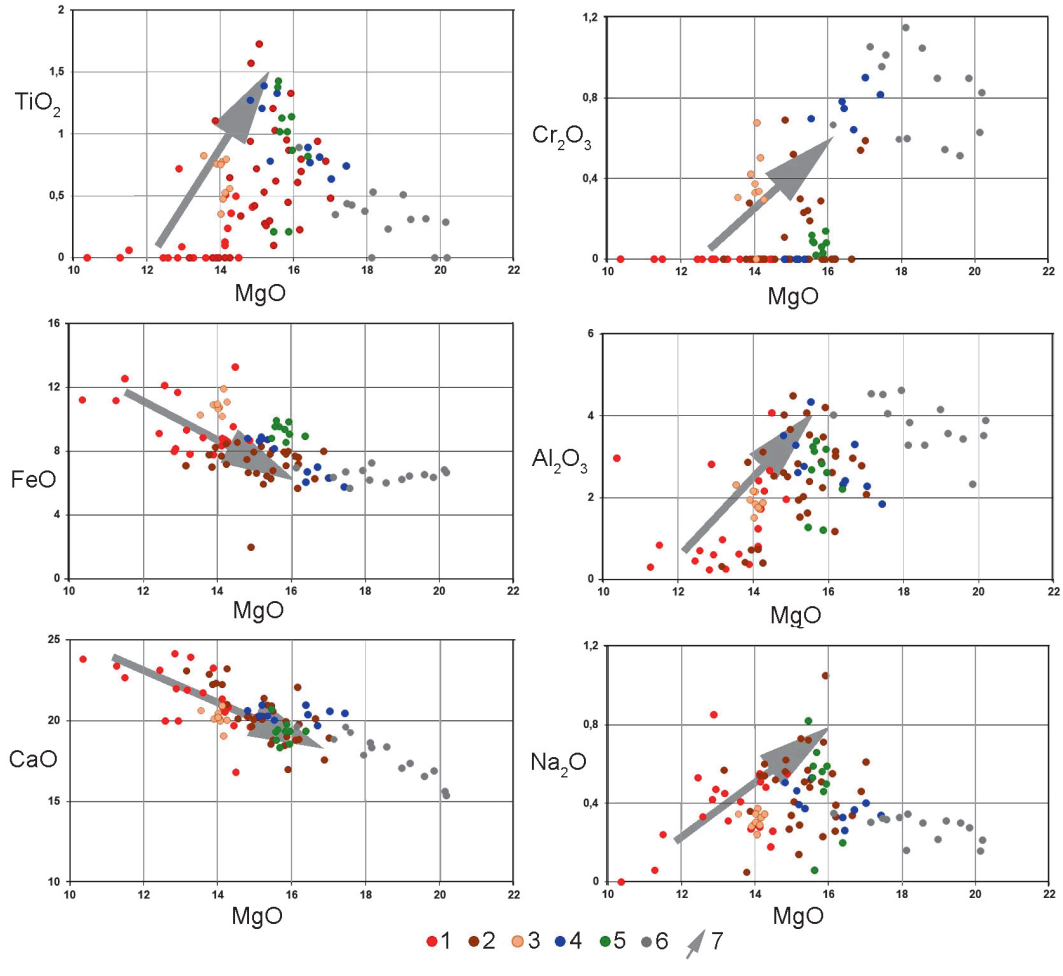

Fig. 5. Binary diagrams for clinopyroxenes from picrite and picrodolerite complexes of the western slope of the Southern Urals. 1 – clinopyroxenes of gabbroids of the Misayelga complex; 2 – clinopyroxenes of the Misayelga complex picrites; 3 – clinopyroxenes of gabbroids and pyroxenites of the Kusinsko-Kopansky complex; 4 – clinopyroxenes from picrites from borehole No. 7; 5 – clinopyroxenes of picrites and picrodolerites of the Lysogorsk complex; 6 – clinopyroxenes from the Ishlinsky picrite complex; 7 – direction of change of components from gabbroids to picrites in clinopyroxenes of the Misayelga complex. 3, 4, 6 after (Sazonova et al., 2011), 5 – author's materials.

No.	SiO_2	TiO_2	Al_2O_3	Cr_2O_3	FeO	MnO	MgO	CaO	Na_2O	K_2O	Total
1	55.58	bdl	1.18	bdl	13.5	0.21	27.93	1.03	0.24	bdl	99.67
2	54.19	bdl	0.99	bdl	14.83	0.14	27.54	1.06	0.32	0.03	99.1
3	55.19	0.28	1.1	0.08	13.83	0.14	27.25	1.29	0.31	bdl	99.47
4	54.76	0.18	1.29	bdl	14.35	0.13	27.53	1.19	0.44	bdl	99.87
5	54.27	0.39	1.77	bdl	13.7	0.12	27.33	1.6	0.38	bdl	99.56
6	55.3	0.38	1.02	0.13	14.31	0.11	26.55	1.28	bdl	bdl	99.08
7	55.05	0.28	1.08	0.19	14.18	0.11	26.72	1.23	0.36	bdl	99.2
8	53.99	0.27	1.47	bdl	15.16	0.11	26.49	1.34	0.33	bdl	99.16
9	53.92	0.36	1.53	bdl	14.67	0.16	27.31	1.36	0.38	bdl	99.69
10	57.06	bdl	0.63	bdl	11.14	0.14	29.87	0.47	0.43	bdl	99.74
11	55.24	0.24	1.01	bdl	13.2	0.09	28.5	0.99	0.18	0.1	99.55
12	54.93	0.42	1.83	0.37	11.99	0.07	28.14	1.17	0.2	bdl	99.12
13	53.15	0.53	1.72	0.69	12.01	0.16	29.96	1.28	0.31	bdl	99.81
14	56.73	bdl	0.88	bdl	12.89	0.12	28.13	0.78	0.43	bdl	99.96
15	55.11	0.15	1.18	bdl	12.95	0.16	28.76	1.03	bdl	bdl	99.34
16	56.46	bdl	0.92	bdl	12.49	0.1	28.63	0.96	0.23	bdl	99.79
17	54.55	0.72	2.15	bdl	13.92	bdl	25.84	1.92	0.44	bdl	99.54
18	54.3	0.45	1.61	bdl	14.14	0.19	27.18	1.51	0.22	bdl	99.6
19	55.91	0.24	1.38	bdl	11.56	0.16	28.76	1.42	0.39	bdl	99.82
20	53.25	0.64	2.39	bdl	14.3	0.18	26.54	2.35	0.13	0.06	99.84
21	55.35	bdl	1.01	bdl	12.92	0.15	29.13	0.98	0.06	bdl	99.6
22	55.54	bdl	0.83	bdl	13.72	0.2	28.56	0.54	bdl	bdl	99.39
23	55.21	0.12	1.03	bdl	14.45	0.19	27.35	1.1	0.1	bdl	99.55
24	55.1	0.11	0.5	bdl	13.75	0.15	28.93	0.62	0.17	bdl	99.33
23	54.04	0.55	1.69	bdl	13.71	0.17	27.55	1.46	0.13	bdl	99.3
26	54.64	0.1	1.63	bdl	14.21	0.19	27.54	0.7	0.21	bdl	99.22
27	54.28	0.15	1.51	bdl	14.17	0.25	28.64	0.31	0.18	0.06	99.55
28	54.31	0.24	0.87	bdl	14.51	bdl	27.83	1.45	0.18	bdl	99.39

Tab. 3. Chemical compositions of orthopyroxene from rocks of the Misayelga complex (wt- %)

No.	Sample No.	Paragenesis	Wood, Banno, 1973	Wells, 1977	Perchuk, 1977	Kretz, 1982	$T°C_{average}$
1	11650	Opx_1	1059	1078	1042	1105	1071
	11650	Cpx_1					
2	11644	Opx_2	1077	1065	1059	1092	1073
	11644	Cpx_2					
3	11641	Opx_3	1069	1098	975	1143	1071
	11641	Cpx_3					
4	11641	Opx_4	960	936	980	973	962
	11641	Cpx_4					

Tab. 4. Crystallization temperatures of pyroxenes from rocks of the ultrabasic horizon of the Misayelga complex

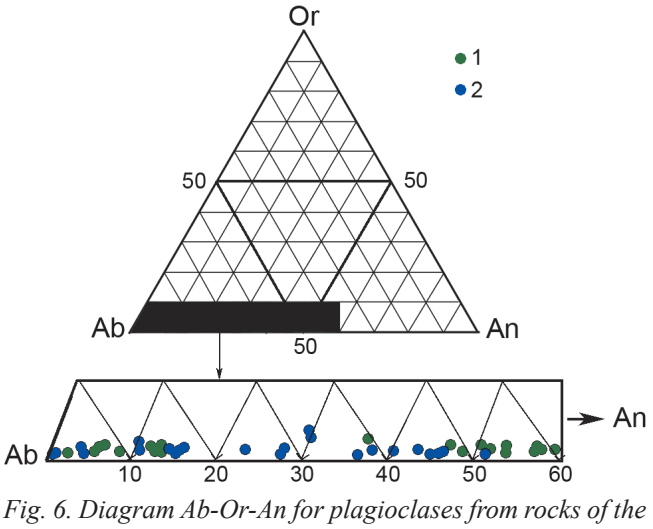

Fig. 6. Diagram Ab-Or-An for plagioclases from rocks of the Misayelga complex: 1 – gabbro horizon; 2 – picrite horizon

by hidden layering, which manifests itself in a change in composition depending on its location in the section. In particular, the Mg # * of biotite in the gabbro horizon varies within 0.23–0.47, and in the picrite horizon it is 0.62–0.87, which indicates the primary magmatic nature of the mineral.

Epidote is present in the form of xenomorphic excretions and granular masses. The chemical composition of the mineral contains: magnesium (0.1–0.19 wt- %), manganese (0.04–0.22 wt- %), titanium (0.3 wt- %), and vanadium (0.67 wt- %). In one case, an epidote fusion was observed – $Ca_{1.97}(Al_{2.20}Fe_{0.74}Mg_{0.02})_{2.96}Si_{3.07}O_{12.00}OH$ with allanite $(Ca_{1.64}Ce_{0.12}La_{0.09}Nd_{0.02})_{1.87}(Al_{1.32}Fe_{0.79}Mg_{0.02})_{2.13}(Si_{3.23}Al_{0.77})_{4.00}O_{12.00}OH$.

Chlorite is found as a secondary mineral in all studied rocks. It is represented by single greenish flakes or

No.	SiO_2	Al_2O_3	FeO	MgO	CaO	Na_2O	K_2O	Total	Composition
1	54.83	27.98	1.56	0.21	9.6	5.15	0.34	99.67	lbd
2	54.32	28.5	0.67	bdl	10.6	5.09	0.36	99.54	lbd
3	64.47	21.68	0.49	bdl	2.57	9.75	0.21	99.17	olc
4	66.53	20.36	bdl	bdl	1.12	11.05	0.14	99.2	ab
5	65.75	20.77	bdl	bdl	2.48	10.35	0.17	99.52	olc
6	58.47	25.94	0.52	bdl	7.2	6.83	0.53	99.49	and
7	67.12	20.58	bdl	bdl	1.06	10.93	0.19	99.88	ab
8	66.69	20.24	bdl	bdl	1.09	11.31	0.09	99.42	ab
9	64.99	21.74	bdl	bdl	2.18	10.23	0.32	99.46	olc
10	54.06	28.29	bdl	bdl	11.91	4.98	0.25	99.49	lbd
11	53.86	29.41	bdl	bdl	11.57	4.79	0.4	100.03	lbd
12	67.14	20.29	bdl	bdl	0.73	11.25	0.11	99.52	ab
13	55.34	28.32	0.37	bdl	9.49	5.58	0.17	99.27	and
14	64.48	22.16	bdl	bdl	2.76	9.79	0.24	99.43	olc
15	55.88	27.5	0.73	0.03	9.12	5.79	0.37	99.42	and
16	67.49	19.49	0.52	0.02	0.43	11.45	0.09	99.49	ab
17	53.22	29.14	0.86	0.05	11.34	4.61	0.34	99.56	lbd
18	52.96	29.5	0.85	bdl	11.62	4.4	0.29	99.62	lbd
19	67.32	20.01	0.33	bdl	0.75	11.02	0.12	99.55	ab
20	65.26	21.77	0.11	0	1.91	10.12	0.43	99.6	olc
21	56.24	27.97	0.19	0.01	9.22	5.89	0.2	99.72	and
22	62.6	23.73	bdl	0.06	4.64	8.72	0.22	99.97	olc
23	56.72	27.66	bdl	0.03	9.3	6.1	0.15	99.96	and
24	55.38	28.18	0.37	bdl	10.25	5.41	0.14	99.73	lbd
25	64.4	21.95	0.45	0.04	3.02	9.49	0.34	99.69	olc
26	56.09	27.3	0.72	bdl	9.24	5.85	0.2	99.4	and
27	63.85	22.01	0.46	bdl	3.14	9.87	0.16	99.49	olc
28	56.23	27.57	0.27	bdl	9.1	5.99	0.16	99.32	and
29	56.61	27.91	0.37	bdl	8.87	6.09	0.11	99.96	and
30	66	21.16	bdl	bdl	2.09	10.26	0.23	99.74	olc
31	56.81	27.22	0.52	bdl	8.23	6.7	0.12	99.6	and
32	61.23	24.78	bdl	bdl	5.55	8.29	0.13	99.98	olc

Tab. 5. A representative sample of the chemical compositions of plagioclases from rocks of the Misayelga complex (wt- %). No. 1–18 – gabbroids, No. 19–32 – picrites. lbd – labradorite, and – andesine, olc – oligoclase, ab – albite.

crystal aggregates with abnormal interference colors that develop along olivine, pyroxene, amphibole, or interstitial space. According to the classification of V.A. Drits and A.G. Kossovskaya (Drits, Kossovskaya, 1991), chlorites belong to Fe-Mg- and Mg-Fe-chlorites of basic igneous rocks. The temperature of their formation, calculated by the formula $T = –61.9229 + 321.9772 \times Al^{IIV}$, published in the work (Kranidiotis, MacLean, 1987), is in the range 157–333 ºC. Between the iron content of chlorites (Fe/(Fe + Mg) f.c.), fluctuating within 0.17–0.67, and the temperature of their formation, there is a clearly manifested inverse relationship, which may indicate the onset of chloritization as an autometamorphic process.

In addition, the association of secondary minerals is represented by talc, the composition of which varies within the range – $(Mg_{2.86}\,Fe_{0.19}\,Al_{0.13})_{3.18}\,Si_{3.82}\,O_{10.00}(OH)_2$ – $(Mg_{2.60}Fe_{0.28}Al_{0.12}Na_{0.08}K_{0.02}Ca_{0.01})_{3.11}Si_{3.89}O_{10.00}(OH)_2$; serpentine – $(Mg_{1.60}\,Fe_{0.25}\,Ni_{0.02})_{1.87}Si_{1.13}O_{4.00}OH$, and calcite – $Ca_{1.00}C_{1.00}O_{3.00}$ – $(Ca_{0.979}Fe_{0.007}\,Sr_{0.005})_{0.99}C_{1.01}O_{3.00}$ – $(Ca_{0.952}\,Mg_{0.021}\,Mn_{0.008}\,Fe_{0.015}\,Sr_{0.005})_{1.00}C_{1.00}\,O_{3.00}$.

Thus, the analysis of the chemical composition of silicates and aluminosilicates that make up the differentiated body of the Misayelga complex made it possible to restore the thermobaric parameters of the crystallization of the melt in the intermediate chamber by calculation methods. In particular, the presence of high-temperature (1472 ºC) intratelluric olivine crystals characterizing the conditions of magma generation at the early stages of fractionation of the melt and olivine crystallizing under the conditions of the intermediate chamber (1050–1183 ºC). The calculated crystallization temperature of pyroxenes indicates that they crystallized together with olivine in the bulk of the rocks, and the established variations in P-T parameters (T = 950–1045 ºC, P = 4.0–7.4 kbar) for plagioclase and amphibole complete the quantitative characterization of high-temperature crystallization processes melt. It should also be emphasized here that the above P-T parameters of crystallization of the melt that formed the intrusive massif make it possible to classify its ultrabasic horizon as picrite complexes of the second type that we identified earlier (Kovalev et al., 2017), and to identify the conditions of its formation with such analogs, as the Shatak volcano-plutonic association (T = 1012–1100 ºC, P = 3–10 kbar) and the layered Kusinsko-Kopansky

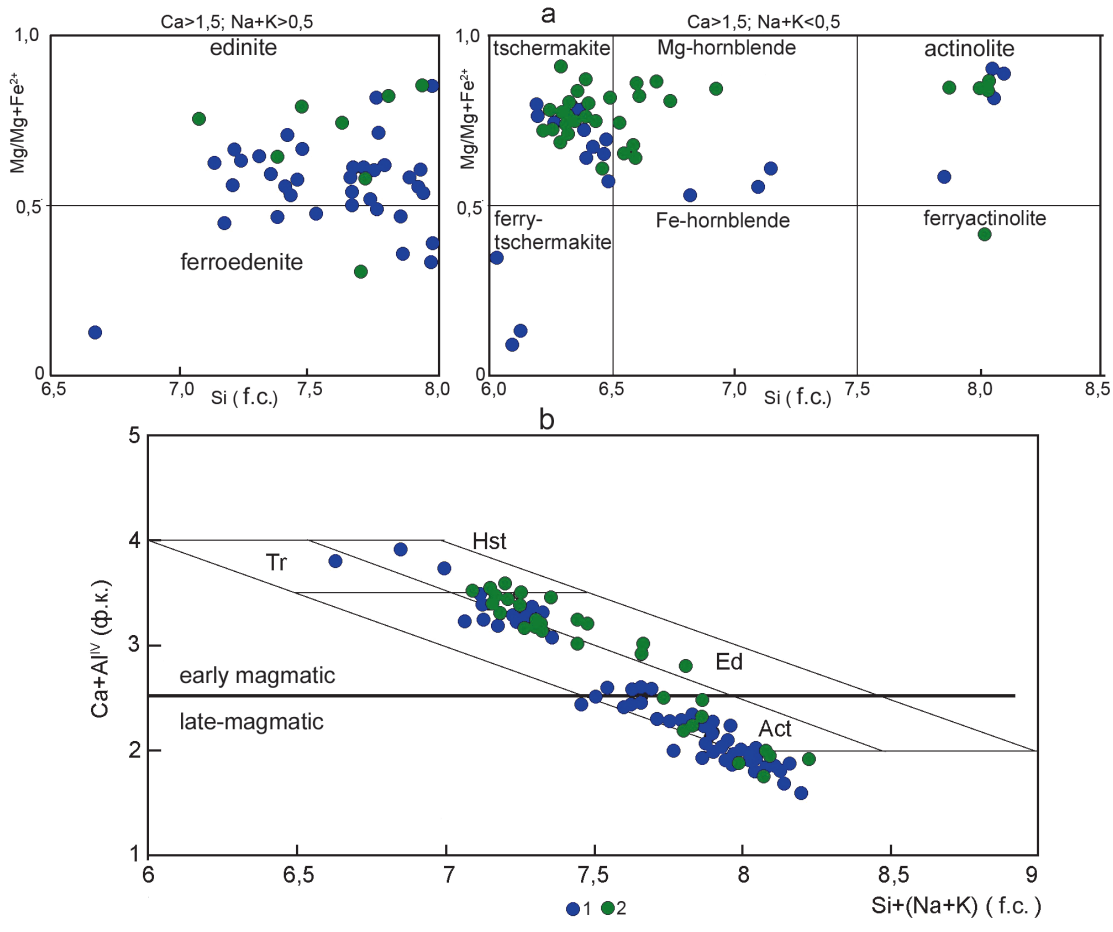

Fig. 7. Classification diagrams (a) and Ca + Al^{IV} – Si + (Na + K) diagram (b) for amphiboles from rocks of the Misayelga complex. a – after (Leake et al., 1997), b – after (Polzunenkov, 2018). Line (Ca + Al^{IV}) = 2.5 after (Giret et al., 1980). Tr – tremolite, Hst – hastingsite, Ed – edinite, Act – actinolite. 1 – picrites; 2 – gabbroids.

complex, represented by picrites from borehole No. 7 (T = 1021–1097 ºC, P = 1–9 kbar) (Kovalev et al., 2017).

Modeling the crystallization process

When describing the simulated processes, the following designations are used: Ol – olivine, Fo – forsterite final, Fa – fayalite final, Cpx – clinopyroxene, Opx – orthopyroxene, Pl – plagioclase, Or – orthoclase, Mgt – magnetite, tiMgt – titanomagnetite, Q – quartz.

Modeling of the crystallization process was carried out using two models: according to the Kh.D. Nathan and K.K. Van Kirk (Nathan, Vankirk, 1978) and the KOMAGMAT software product, version 5.2.2, at P – 0.001 kbar; lg fO_2 – –14.51; dQFM – –8 (Ariskin et al., 1986, 1993; Frenkel et al., 1988). The calculated weighted average composition of the intrusive body (wt- %) was taken as the melt: SiO_2 – 48.23, TiO_2 – 1.87, Al_2O_3 – 8.4, FeO – 17.11, MnO – 0.2, MgO – 14.74, CaO – 8.32, Na_2O – 1.37, K_2O – 0.62 (Alekseev et al., 2000). After obtaining the results of modeling and plotting crystallization diagrams (Fig. 8), two possible mechanisms of intrachamber differentiation of the melt were analyzed: equilibrium crystallization according to the Kh.D. Nathan and K.K. Van Kirk (Nathan, VanKirk, 1978) during gravitational fractionation of the solid phase and fractional[2] crystallization calculated using the software product COMAGMAT (Ariskin et al., 1986, 1993; Frenkel et al., 1988; Ariskin, Barmina, 2004) with directional crystallization (Sharkov, 1980). When constructing the models, the following provisions were postulated: the absence of convection, the latent heat of crystallization was not taken into account, the fixed heat transfer was 20 deg/year, the size of the crystals was 1 mm. The correctness of the model was determined by the degree of its correspondence to the real section of the body.

Crystallization of the melt according to the algorithm of Kh.D. Nathan and K.K. Van Kirk (Nathan, VanKirk, 1978) (Fig. 8, a) begins with Ol at a temperature of 1304 ºC, after the separation of about 24 % of crystals, tiMgt appears on the liquidus, and at a temperature of 1207 ºC, Cpx + tiMgt association with a small amount of Ol crystallizes. As a result, when the temperature drops to 1185 ºC, about 48 % of the melt volume is represented by the Ol + Cpx + tiMgt association. In the temperature range 1185–1143 ºC Pl + Cpx + Opx + Mgt + Ol association crystallizes in the proportions shown in the diagram (Fig. 8, a). The melt composition in this interval is probably close to subeutectic (Yaroshevsky, 1964), which is displayed on the diagram in the form of

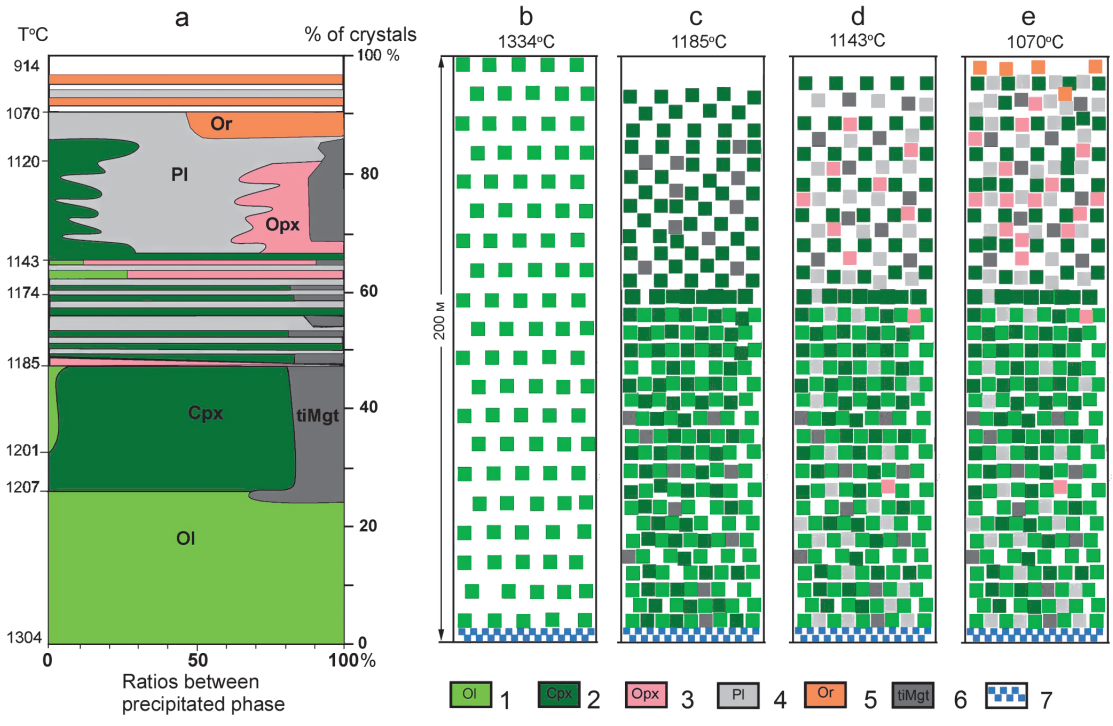

Fig. 8. Diagram of crystallization of the weighted average composition of the Misayelga complex according to Kh.D. Nathan and K.K. Van Kirk (Nathan, VanKirk, 1978) and models of gravitational deposition of crystals. The area of 1 digit is 1 % of the crystalline phase. Due to the peculiarities of the graphic display, the accuracy of the image of the amount of the crystalline phase in the volume of the melt is ± 5–10 %. 1 – olivine; 2 – clinopyroxene; 3 – orthopyroxene; 4 – plagioclase; 5 – orthoclase; 6 – titanomagnetite; 7 – endocontact zone.

alternating bands representing crystallization from the melt of one of the minerals. Then the Pl + Opx + Cpx + tiMgt association crystallizes, alternating with Or + Pl + Q, which completes the process of formation of the intrusive body.

Using the mechanism of gravitational fractionation of the solid phase, the changes in the density and viscosity of the melt during crystallization and the rate of deposition of minerals were calculated for individual temperature stages of the formation of the massif. The density was calculated according to the additive scheme (Appen, 1974):

$$\frac{100}{d} = \frac{Vj}{dj}, \quad (1)$$

where d is the density, V_j is the weight percent of the melt components, d_j are the coefficients characteristic of each component.

The values of the viscosity of the basalt melt, depending on the temperature, were determined according to the data of M.P. Volarovich, published in the work of R. Müller and S. Saxena (Müller, Saxena, 1980). The deposition rate of minerals was calculated using the Stokes formula:

$$V = \frac{2gr^2(\Delta\rho)}{9\eta}, \quad (2)$$

where V is the velocity, g is the gravity acceleration, r is the radius, $\Delta\rho$ is the difference in the density of the particle and the liquid, η is the viscosity, which took into account the change in the viscosity and density of the melt depending on the change in temperature.

Analyzing the dynamics of the formation of a differentiated body of the Misayelga complex from the point of view of gravitational fractionation, on the basis of the obtained results of modeling equilibrium crystallization and calculated rates of mineral deposition, diagrams were constructed that depict the fractionation of the solid phase for various temperature sections (Fig. 8, b, c, d, e).

With the chemical homogeneity of the melt, crystallization of Ol begins at a temperature of 1330 ºC (83–90 % Fo) in the entire volume of the intermediate chamber (Fig. 8, b). At a gravitational precipitation rate of 6.35–5.8 m / year, its complete settlement will be completed in an average of 30–35 years (with a crystal size of 1 mm), taking into account the change in the density of the melt. Further (at a temperature of 1207 ºC), Cpx and tiMgt are added to Ol, which also precipitate due to the fact that their density is higher than that of the melt, but the rate of their deposition is much lower. As a result, about 50 % of the melt volume crystallizes with the formation of a horizon, the bottom of which is composed of olivine cumulates, and the upper part is Cpx-tiMgt. Since the movement of crystals in the melt under the action of gravitational forces is directed from top to bottom, then after crystallization of 50 % of the melt volume, we can say that more than half of

the vertical section of the body will be represented by rock, the structure of which is determined by a pseudo-frame of cumulus minerals and a certain amount of interstitial melt, and also by the presence of crystals of early minerals in suspension in the volume of the residual melt (Fig. 8, c).

After the separation of 50 % of the crystals, the density of the residual melt is 2.53 g/cm^3, and Pl, Cpx, Opx with small Ol and tiMgt appear on the liquidus. It should be noted that the deposition rates of minerals at this stage are low, and if relatively efficient fractionation can be assumed for Ol and pyroxenes, then the Pl crystals should practically remain in a suspended state. That is, a horizon is formed here, the rocks of which are composed of cumulus minerals (Cpx + Ol) with a slight increase in their amount from top to bottom along the section, with an almost constant Pl content throughout the section of the interval. Then, at 30 % of the residual melt, the Pl + Opx + tiMgt association begins to crystallize (Fig. 8, d), but since some of the previously precipitated crystals (Pl, in particular) remain in a suspended state, and the release of this association occurs when the temperature decreases by 20º, a significant amount of the crystalline phase per unit volume of the melt will complicate (or make impossible) the process of gravitational fractionation, and as a result, this mechanism ceases to play any significant role in the process of mineral redistribution.

Thus, as a result of the action of the gravitational fractionation mechanism, we obtain the following schematic section of the body: the lower horizon of Ol and Ol + Cpx cumulates, passing into a horizon with a weakly manifested accumulation of pyroxenes in the lower parts and an almost uniform distribution of Pl, which ends in plagioclase-bipyroxene rocks without sliding – any noticeable fractionation, with streaks and segregations of acidic (plagiogranite) material (Fig. 8, e). It should also be noted here that the described model will be implemented only if a significant compaction of the crystalline "sediment" in the lower horizons (filter-pressing) is allowed, otherwise, after crystallization of 50 % of the melt volume, the internal structure of the massif will be characterized by a pseudo-frame of minerals cumulus, occupying almost the entire volume of the magma chamber, and gravitational fractionation here becomes impossible.

Fractional crystallization of the melt, calculated using the KOMAGMAT software product, is shown in Figure 9. As can be seen from the diagram, the first precipitated phase at a temperature of 1380 ºC will be Ol (77–85 % Fo), to which at T – 1164 ºC Cpx is added, as a result of which 40 % of the melt volume is represented by the bimineral Ol + Cpx association. Further, in the temperature range 1139–904 ºC, the Cpx + Pl + Pg + tiMgt + Ilm association stands out. The remaining 10 % of the melt is interstitial material, the crystallization of which is not described within the framework of the given model.

Analyzing the results obtained using the directed crystallization mechanism, it should be noted that the constructed diagram (Fig. 9, a) is in fact a graphical display of the process of the crystallization front advancing with the emerging liquidus minerals as the temperature decreases. The mechanism of directed

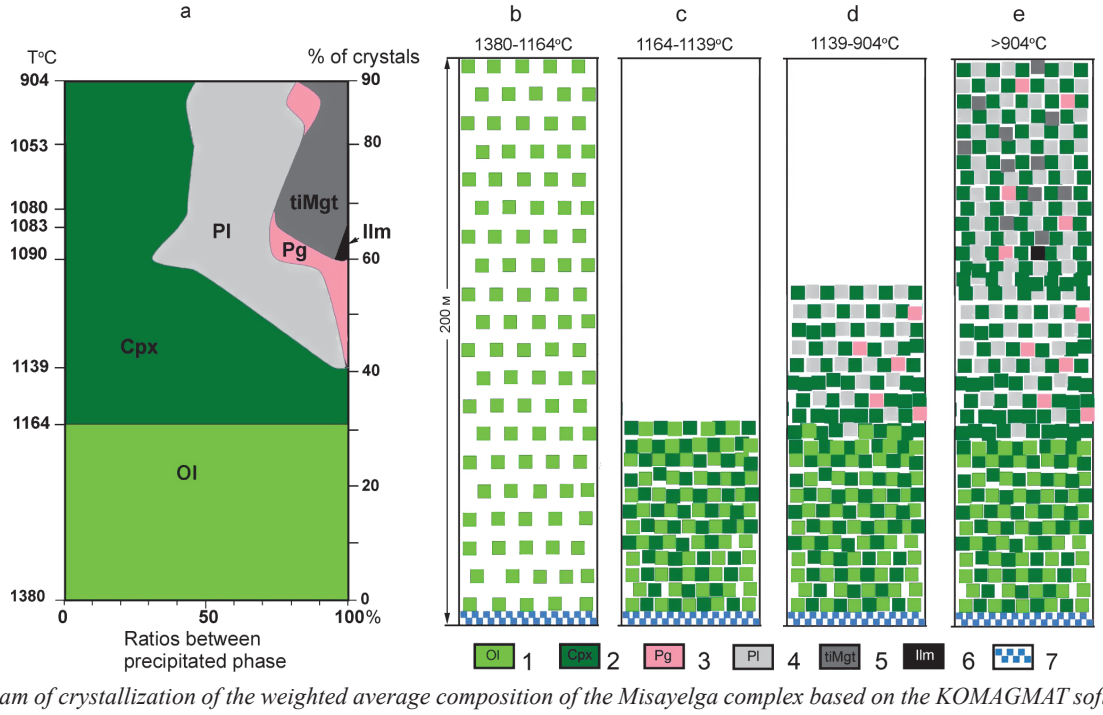

Fig. 9. Diagram of crystallization of the weighted average composition of the Misayelga complex based on the KOMAGMAT software product and the directional crystallization model. The area of 1 digit is 1 % of the crystalline phase. Due to the peculiarities of the graphic display, the accuracy of the image of the amount of the crystalline phase in the volume of the melt is ± 5–10 %. 1 – olivine; 2 – clinopyroxene; 3 – pigeonite, 4 – plagioclase; 5 – titanomagnetite; 6 – ilmenite; 7 – endocontact zone

crystallization is considered in detail by E.V. Sharkov (Sharkov, 1980), its essence lies in the fact that the crystallization of the internal parts of the intrusive massif occurs by moving upward of the solidification front (crystallization zone), consisting of crystalline phases of liquidus, and the bulk of the residual melt is squeezed out into the main volume, enriching it with low-temperature components.

The fundamental point in the implementation of this model, in our opinion, is the initial stage of the formation of the crystallization front. If we assume that it is formed as a continuation of the endocontact zone directed from the contact into the massif, then in this case we must assume the chemical heterogeneity of the melt, which is practically unrealizable within the framework of existing petrological models. Therefore, in our model, at the initial stages (temperature range 1380–1164 ºC in Fig. 9, a, b), Ol crystallizes in the entire volume of the melt during the implementation of the gravitational fractionation mechanism due to the fact that the solidification front has not yet formed under these conditions. It should be emphasized that the temperature range of crystallization of one Ol according to this model is 216 ºC, while according to the first model it is 97 ºC (Fig. 9, a), due to which the gravitational jigging of Ol will be more "effective" (Fig. 9, c). Further, using the process of directed crystallization as a mechanism that determines the dynamics of the formation of the intrusive body of the Misayelga complex, we have the following scheme of the formation of the massif:

- As the formed crystallization front advances (from bottom to top), the liquidus mineral, Cpx, is released (Fig. 9, c), as a result of which the lower horizon of the intrusive body will be represented by an ultrabasic rock composed of Ol + Cpx associations with an insignificant amount of interstitial melt;

- Further on the liquidus Cpx + Pl + Pg association appears (Fig. 9, d), to which tiMgt with a small amount of Ilm joins at a temperature of 1090 ºC, in the proportions shown in Fig. 9, e. Thus, the formed upper horizon of the intrusive body will be represented by typical gabbroids.

Results and discussion

As noted above, the correctness of the results of the computational model is determined by the degree of its correspondence to the real section of the body. Figure (10, a) shows a real section of the body, built by sketching thin sections, and model sections built according to: the algorithm of H.D. Nathan and K.K. Van Kirk (Nathan, VanKirk, 1978) (Fig. 10, b) – model 1; the KOMAGMAT software product (Fig. 10, c) – model 2. The first thing that should be noted is that it was possible to obtain a two-term structure of the sections using both model 1 and model 2. Comparative analysis of a real body section with model 1 shows that the model section is significantly different from the real one. In the model section, the presence of Ol crystals is observed throughout the ultramafic horizon and the presence of a significant amount of Opx in the gabbro interval, while in the real section of the body, the upper part of the ultramafic horizon is composed of olivine-free Cpx + Opx rocks, and is absent in the gabbro horizon. The structure of the model section 2 corresponds more to the real one, since it highlights the lower horizon enriched with Ol, which is replaced by Cpx+Opx rocks up the section and in the upper part corresponds to gabbroids with a small amount of pigeonite.

In addition to comparing the internal structure of bodies, it seems important to analyze the chemical composition of the main minerals of the early generation during the evolution of the melt. Figure 11 shows diagrams for Ol (Fig. 11, a, b) and Cpx (Fig. 11, c), which show changes in the chemical composition of minerals according to the calculated models, the parameters of which are described above, and real existing minerals. As can be seen from the analysis of the diagrams, the chemical composition and crystallization temperature of Ol, calculated by the algorithm of Kh.D. Nathan and K.K. Van Kirk, to a large extent differ from the existing ones, which, together with the structural features of the section described above, makes it possible to further not

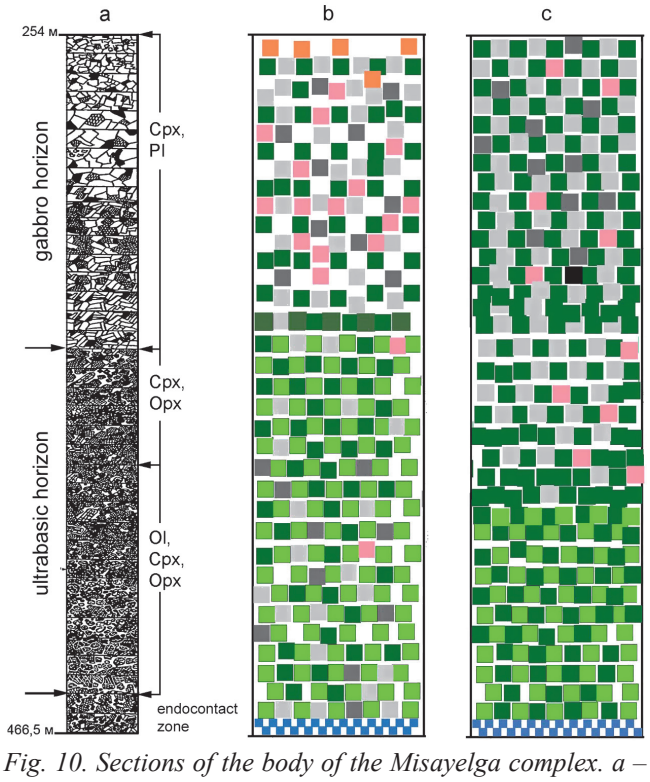

Fig. 10. Sections of the body of the Misayelga complex. a – a real section of the body, built by sketching thin sections; b – model section, built when modeling the crystallization process according to the algorithm of Kh.D. Nathan and K.K. Van Kirk (Nathan, VanKirk, 1978); c – a model section constructed when modeling the crystallization process using the COMAGMAT software product (Ariskin, Barmina, 2004). For legend see Fig. 8 and Fig. 9

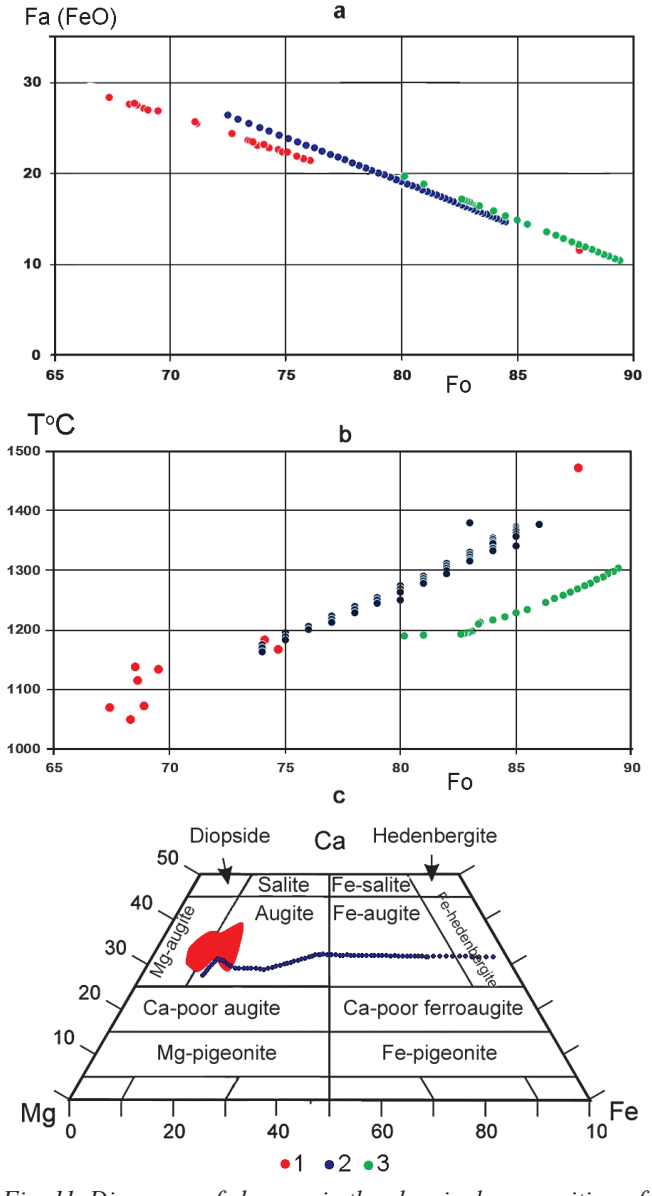

Fig. 11. Diagrams of changes in the chemical composition of olivines and clinopyroxenes in the course of melt evolution. 1 – actual minerals, 2 – calculated using the COMAGMAT software product, 3 – calculated using the Kh.D. Nathan and K.K. Van Kirk. In diagram «a», Fa-Fo parameters are used for model compositions, and FeO_{Ol}–Fo for real ones

consider this model as adequately describing the real conditions of the formation of the differentiated body of the Misayelga complex. Changes in the chemical composition and crystallization temperature of Ol calculated using the KOMAGMAT software product, as can be seen from the diagrams (Fig. 11, a, b), are, in fact, a continuation of real trends in the high-temperature region. At the same time, the rocks of the complex lack Ol with a forsterite endpoint content of more than 77 % (Table 1). There can be several explanations: from the simplest – the relatively small statistics of microprobe measurements, to the complex – the change in the chemical composition of Ol as a result of equilibrium crystallization, while we are aware of the values of the crystallization rate during equalizing diffusion in the melt and the crystallizing phase.

The chemical composition of the melt, which we calculated as the weighted average amount of oxides (see above), is also, most likely, close to the real melt, since the average contents of MgO in the upper body with n = 12 analyzes is 12.93 wt- %, which slightly differs from the amount of MgO in the weighted average composition of the lower body – 14.74 wt- %. With such an amount of magnesium oxide, there will be no fundamental differences in the content of the forsterite endpoint and the crystallization temperature of Ol from those shown in Fig. 11, a, b. Thus, the question of the presence of high-temperature Ol in the calculated models remains open. The situation is different with the composition of clinopyroxene. As can be seen from the classification diagram (Fig. 11, c), at the initial stages of crystallization, Cpx is formed, which is close in composition to that actually existing in the rocks of the complex. Further evolution of the chemical composition of Cpx towards Fe-hedenbergite is actually characterized by a change in association, in which amphibole will crystallize instead of Cpx, which is not included in the model calculations, but its calculated maximum crystallization temperature is 1045 ºC (see above), which is very close to the temperature range of crystallization Cpx (1071–1073 ºC), i.e. changing the association is a very real process.

Thus, the comparative analysis of the modeling results with the structure of the real section of the intrusive body of the Misayelga complex indicates that the most probable mechanism of its formation was directional crystallization with gravitational deposition of Ol at the initial stages of the formation of the massif.

Conclusion

As a result of the analysis of the chemical composition of silicates and aluminosilicates composing the differentiated body of the Misayelga complex, the thermobaric parameters of the crystallization of the melt in the intermediate chamber were characterized by calculation methods.

The presence of high-temperature (1472 °C) intratelluric olivine crystals characterizing the process in the magma generation chamber and olivine crystallizing under the conditions of the intermediate chamber (1050–1183 °C) has been established. The calculated crystallization temperature of pyroxenes indicates that they crystallized together with olivine in the bulk of the rocks, and the established variations in P-T parameters (T = 950–1045 °C, P = 4.0–7.4 kbar) for plagioclase and amphibole complete the quantitative characteristics of high-temperature crystallization processes melt.

It is shown that the calculated P-T parameters of crystallization of the melt that formed the intrusive massif make it possible to classify its ultrabasic horizon

as picrite complexes of the second type that we identified earlier.

Modeling of the crystallization process, carried out using two models – according to the algorithm of Kh.D. Nathan and K.K. Van Kirk and the KOMAGMAT software product, and two mechanisms of intrachamber differentiation – equilibrium crystallization during gravitational fractionation of the solid phase and fractional crystallization during directional crystallization, made it possible to establish that the most probable mechanism for the formation of a differentiated body of the Misayelga complex was directional crystallization with gravitational deposition of olivine at the initial stages the process of the formation of the array.

Acknowledgements

The research was carried out within the framework of the State Assignment of the IG UFIC RAS (project No. 0252-2017-0012).

The authors are grateful to V.A. Kotlyarov for his highly professional analysis of the minerals and are also grateful to the anonymous reviewers for helpful comments which improved the work.

References

Aitcheson, S.J., Forrest, A.H. (1994). Quantification of crustal contamination in open magmatic systems. *Journal of Petrology*, 35, pp. 461–488. https://doi.org/10.1093/petrology/35.2.461

Alekseev A.A. (1984). Riphean-Vendian magmatism of the western slope of the Southern Urals. Moscow: Nauka, 136 p. (In Russ.)

Alekseev A.A., Alekseeva G.V., Kovalev S.G. (2000). Layered intrusions of the western slope of the Urals. Ufa: Gilem, 188 p. (In Russ.)

Appen A.A. (1974). Glass chemistry. Leningrad: Khimiya, 125 p. (In Russ.)

Ariskin A.A., Barmina G.S. (2004). COMAGMAT: Development of a magma crystallization model and its petrologic applications. *Geochemistry International*, 42(Suppl. 1), pp. 1–157.

Ariskin A.A., Barmina G.S. (2000). Modelirovanie fazovykh ravnovesiy pri kristallizatsii bazal'tovykh magm. Moscow: Nauka, 363 p. (In Russ.)

Ariskin A.A., Barmina G.S., Frenkel M.Yu. (1986). Computer simulation of basalt magma crystallization at a fixed oxygen fugacity. *Geochem. Int.*, 24(5), pp. 92–100. (In Russ.)

Ariskin A.A., Frenkel M.Yu., Barmina G.S., Nilsen R. (1993). Comagmat: a Fortran program to model magma differentiation processes. *Comput. Geosci.*, 19(8), pp. 1155–1170. https://doi.org/10.1016/0098-3004(93)90020-6

Beattie P. (1993). Olivine-melt and orthopyroxene-melt equilibria. *Contributions to Mineralogy and Petrology*, 115(1), pp. 103–111. https://doi.org/10.1007/BF00712982

Blundy J.D., Holland T.J.B. (1990). Calcic amphibole equilibria and a new amphibole-plagioclase geothermometer. *Contrib Mineral Petrol*, 104(2), pp. 208–224. https://doi.org/10.1007/BF00306444

Bohrson W.A., Spera F.J. (2001). Energy-Constrained Open-System Magmatic Processes II: Application of energy-constrained assimilation–fractional crystallization (EC-AFC) model to magmatic systems. *J. Petrol.*, 42(5), pp. 1019–1041. https://doi.org/10.1093/petrology/42.5.1019

Bohrson W.A., Spera F.J. (2003). Energy-constrained opensystem magmatic processes 4; Geochemical, thermal and mass consequences of Energy-Constrained Recharge, Assimilation and Fractional Crystallization (EC-RAFC). *Geochem. Geophys. Geosyst.*, 4(2). https://doi.org/10.1029/2002GC000361

Bowen N.L. (1928). The Evolution of the Igneous Rocks. Princeton University Press, Princeton, 334 p.

Bychkov D.A., Koptev-Dvornikov E.V. (2005). Cri-Minal program for modeling the melt-solid phase equilibrium for a given gross composition of the system. *Proc. Conf.: Ultramafic-mafic complexes of folded areas of the Precambrian*. Ulan-Ude: BurNTs SB RAS, pp. 122–123. (In Russ.)

Campbell F.E., Roeder P. (1968). The stability of olivine and pyroxene in the Ni-Mg-Si-O system. *Am. Mineralog*, 53, pp. 257–268.

De Hoog Jan C.M., Gall Louise, David H.C. (2010). Trace-element geochemistry of mantle olivine and application to mantle petrogenesis and geothermobarometry. *Chemical Geology*, 270(1–4), pp. 196–215. https://doi.org/10.1016/j.chemgeo.2009.11.017

DePaolo D.J. (1981). Trace element and isotopic effects of combined wallrock assimilation and fractional crystallization. *Earth and Planetary Science Letters*, 53(2), pp. 189–202. https://doi.org/10.1016/0012-821X(81)90153-9

Drits V.A., Kossovskaya A.G. (1991). Clay minerals: micas, chlorites. Moscow: Nauka, 176 p. (In Russ.)

Erofeeva, K.G., Stepanova, A.V., Samsonov, A.V. et al. (2019) 2.4 Ga Mafic Dikes and Sills of Northern Fennoscandia: Petrology and Crustal Evolution. *Petrology*, 27, pp. 17–42. https://doi.org/10.1134/S0869591119010016

Frenkel M.Ya., Yaroshevskiy A.A., Ariskin A.A., et al. (1988). Dynamics of intrachamber differentiation of basic magmas. Moscow: Nauka, 216 p. (In Russ.)

Fuchs L.H., Olsen E., Jensen K.J. (1973). Mineralogy, Mineral-Chemistry, and Composition of the Murchison (C2) Meteorite. *Smithson. Contrib. Earth Sci.*, 10, pp. 1–39. https://doi.org/10.5479/si.00810274.10.1

Gillis K.M., Snow J.E., Klaus A., Abe N., Adriao A.B., Akizawa N., Ceuleneer G., Cheadle M.J., Faak K., Falloon T.J., Friedman S.A., Godard M., Guerin G., Harigane Y., Horst A.J., Hoshide T., Ildefonse B., Jean M.M., John B.E., Koepke J., Machi S., Maeda J., Marks N.E., McCaig A.M., Meyer R., Morris A., Nozaka T., Python M., Saha A., Wintsch R.P. (2014) Primitive layered gabbros from fastspreading lower oceanic crust. *Nature,* 505, pp. 204–207. https://doi.org/10.1038/nature12778

Giret A., Bonin B., Leger J.M. (1980). Amphibole compositional trends in oversaturated alkaline plutonic ring-complexes. *The Canadian Mineralogist*, 18, pp. 481–495.

Humphreys M.C.S (2011) Silicate liquid immiscibility within the crystal mush: evidence from Ti in plagioclase from the Skaergaard intrusion. *J Petrol.,* 52, pp. 147–174. https://doi.org/10.1093/petrology/egq076

Kovalev S.G. (1996). Differentiated diabase-picrite complexes of the western slope of the Southern Urals. Ufa: IG UNTs RAS, 99 p. (In Russ.)

Kovalev S.G. (2011). New data on the geochemistry of diabase-picrite magmatism on the western slope of the Southern Urals and the conditions for its formation. *Litosfera = Lithosphere (Russia)*, 2, pp. 68–83. (In Russ.)

Kovalev S.G., Kovalev S.S., Vysotskiy S.I. (2018). Noble metal geochemical specialization of the Mesoproterozoic magmatic complexes of the Bashkirian meganticlinorium and the eastern margin of the East European platform. *Litosfera = Lithosphere (Russia)*, 18(2), pp. 295–313. (In Russ.) https://doi.org/10.24930/1681-9004-2018-18-2-295-313

Kovalev S.G., Puchkov V.N., Vysotskiy S.I., Kovalev S.S. (2017). Conditions for the formation of igneous rocks during the plume process (on the example of the western slope of the Southern Urals). *DAN*, 475(2), pp. 171–175. (In Russ.) https://doi.org/10.7868/S0869565217200129

Kranidiotis P., MacLean W.H. (1987). Systematic of Chlorite Alteration at the Phelps Dodge Massive Sulfide Deposit, Matagami, Quebec. *Economic Geology*, 82(7), pp. 1808–1911. https://doi.org/10.2113/gsecongeo.82.7.1898

Kretz R. (1982). Transfer and exchange equilibria in a portion of the pyroxene quadrilateral as deduced from natural and experimental data. *Geochimica et Cosmochimica Acta*, 46(3), pp. 411–422. https://doi.org/10.1016/0016-7037(82)90232-0

Layered Intrusions. (2015). Eds: Charlier B., Namur O., Latypov R., Tegner C. Springer, 748 p.

Leak B.E. (1978). Nomenclature of amphiboles. *Miner. Mag.*, 42(324), pp. 533–563. https://doi.org/10.1180/minmag.1978.042.324.21

Lennykh V.I., Petrov V.I. (1978). Picrites of the Taratash complex. *Trudy Il'men. gos. zapoved.*, vol. 17, pp. 45–52. (In Russ.)

Lepage L.D. (2003). ILMAT: an excel worksheet for ilmenite-magnetite geothermometry and geobarometry. *Comput. Geosci*., 29(5), pp. 673–678. https://doi.org/10.1016/S0098-3004(03)00042-6

Leuthold J, Blundy J.D, Holness M.B, Sides R. (2014) Successive episodes of reactive liquid flow through a layered intrusion (Unit 9, Rum Eastern Layered Intrusion, Scotland). *Contrib. Mineral. Petrol.,* 168, pp. 1–27. https://doi.org/10.1007/s00410-014-1021-7

Lindsley D.H., Spencer K.J. (1982). Fe-Ti oxide geothermometry: Reducing analyses of coexisting Ti-magnetite (Mt) and ilmenite (Ilm). *American Geophysical Union*, 63(18), p. 471.

Loucks Robert R. (1996). A precise olivine-augite Mg-Fe-exchange geothermometer. *Contrib Mineral. Petrol*., 125(2–3), pp. 140–150. https://doi.org/10.1007/s004100050211

Miyamoto M., Furuta T., Fujii NMcKay., D.S., Lofgren G.E., Duke

M.B. (1993). The Mn-Fe negative correlation in olivines in ALHA 77257 ureilite. *Journal of Geophysical Research*, 98(E3), pp. 5301–5307. https://doi.org/10.1029/92JE02943

Myuller R., Saksena S. (1980). Chemical petrology. Moscow: Mir, 516 p. (In Russ.)

Namur O, Charlier B, Toplis M.J, Higgins M.D, Liégeois J-P, Vander Auwera J. (2010) Crystallization sequence and magma chamber processes in the ferrobasaltic Sept Iles layered intrusion, Canada. *J. Petrol.,* 51, pp. 1203–1236. https://doi.org/10.1093/petrology/egq016

Nathan H.D., Vankirk C.K. (1978). A model of magmatic crystallization. *Petrol*., 19(1), pp. 66–94. https://doi.org/10.1093/petrology/19.1.66

Nielsen R.L. (1985). EQUIL: a program for the modeling of low-pressure differentiation processes in natural mafic magma bodies. *Computers & Geosciences*, 11, pp. 531–546. https://doi.org/10.1016/0098-3004(85)90084-6

Nielsen R.L. (1988). TRACE FOR: A program for the calculation of combined major and trace-element liquid lines of descent for natural magmatic systems. *Computers & Geosciences*, 14, pp. 15–35. https://doi.org/10.1016/0098-3004(88)90050-7

Nosova, A.A., Sazonova, L.V., Kargin, A.V. et al. (2012) Mesoproterozoic within-plate igneous province of the western urals: Main petrogenetic rock types and their origin. *Petrology,* 20, pp. 356–390. https://doi.org/10.1134/S086959111204008X

Perchuk L.L., Saxena S.K and Bhattacharji S. (1977). Thermodynamic control of metamorphic processes in Energetics of Geological Processes. New York: Springer.https://doi.org/10.1007/978-3-642-86574-9

Polzunenkov G.O. (2018). Evaluation of P-T and fO2 conditions of crystallization of monzonitoids of the Velitkenai granite-migmatite massif (Arctic Chukotka) based on mineral thermobaro- and oxybarometry data. *Tikhookeanskaya geologiya*, 37(5), pp. 97–111. (In Russ.)

Powell R. (1984). Inversion of the assimilation and fractional crystallization (AFC) equations; characterization of contaminants from isotope and trace element relationships in volcanic suites. *Journal of Geological Society of London*, 141(3), pp. 447–452. https://doi.org/10.1144/gsjgs.141.3.0447

Roedder P.L., Emslie R.F. (1970). Olivine-liquid equilibrium. *Contributions to Mineralogy and Petrology*, 29(4), pp. 275–289. https://doi.org/10.1007/BF00371276

Sazonova L.V., Nosova A.A., Larionova Yu.O., Kargin A.V., Kovalev S.G. (2011). Mesoproterozoic picrites of the eastern margin of the East European Platform and the Bashkirian meganticlinorium: petrogenesis and compositional features of olivine and clinopyroxene. *Litosfera = Lithosphere (Russia)*, 3, pp. 64–83. (In Russ.)

Sharkov E.V. (1980). Petrology of layered intrusions. Leningrad: Nauka, 120 p. (In Russ.)

Spera F.J., Bohrson W.A. (2001). Energy-constrained opensystem magmatic processes, 1, General model and energyconstrained assimilation and fractional crystallization (ECAFC) formulation. *J. Petrol*., 42(5), pp. 999–1018. https://doi.org/10.1093/petrology/42.5.999

Spera F.J., Bohrson W.A. (2002). Energy-constrained opensystem magmatic processes 3. Energy-constrained recharge, assimilation, and fractional crystallization (EC-RAFC). *Geochemistry Geophysics Geosystems*, 3(12), pp. 1–20. https://doi.org/10.1029/2002GC000315

Spera F.J., Bohrson W.A. (2004). Open-system magma chamber evolution: an energy-constrained geochemical model incorporating the effects of concurrent eruption, recharge, variable assimilation and fractional crystallization (EC-E'RA FC). *Journal of Petrology*, 45(12), pp. 2459–2480. https://doi.org/10.1093/petrology/egh072

Toramaru A, Matsumoto M. (2012) Numerical experiment of cyclic layering in a solidified binary eutectic melt. *J. Geophys. Res.,* 117, B02209. https://doi.org/10.1029/2011JB008204

Wager L.P., Brown G. (1968). Layered igneous rocks. Edinburgh; London: Oliver & Boyd, 588 p.

Wells P.R.A. (1977). Pyroxene thermometry in simple and complex systems. *Contributions to Mineralogy and Petrology*, 62(2), pp. 129–139. https://doi.org/10.1007/BF00372872

Wood B.J., Banno S. (1973). Garnet-orthopyroxene and orthopyroxene-clinopyroxene relationships in simple and complex systems. *Contributions to Mineralogy and Petrology*, 42(2), pp. 109–124. https://doi.org/10.1007/BF00371501

Yaroshevskiy A.A. (1964). The principle of zone melting and its application in solving some geochemical issues. *Proc. Conf.: Chemistry of the Earth's Crust*, vol. 2. Moscow: Nauka, pp. 55–62. (In Russ.)

About the Authors

Sergey G. Kovalev – Director, DSc (Geology and Mineralogy)

Institute of Geology – Subdivision of the Ufa Federal Research Centre of the Russian Academy of Sciences

16/2 Karl Marx st., Ufa, 450077, Russian Federation

Sergey S. Kovalev – Junior Researcher

Institute of Geology – Subdivision of the Ufa Federal Research Centre of the Russian Academy of Sciences

16/2 Karl Marx st., Ufa, 450077, Russian Federation

Manuscript received 27 April 2021;
Accepted 8 September 2021;
Published 30 November 2021